Journal of
Synchrotron Radiation

ISSN 0909-0495

Received 30 January 2008
Accepted 16 May 2008

Analyser-based tomography images of cartilage

Ahi S. Issever,[a,b]* Gerd Diederichs,[a,b] Sharmila Majumdar,[b] Patrik Rogalla,[a] Bernd K. Hamm,[a] Axel Lange,[c] Michael Harwardt,[c] Manfred P. Hentschel[c] and Bernd R. Mueller[c]

[a]Department of Radiology, Charité Campus Mitte, Universitaetsmedizin Berlin, Berlin, Germany, [b]Musculoskeletal and Quantitative Imaging Research Group, Department of Radiology and Biomedical Imaging, University of California, San Francisco, CA, USA, and [c]Federal Institute for Materials Research and Testing, Berlin, Germany. E-mail: ahi-sema.issever@charite.de

Analyser-based imaging expands the performance of X-ray imaging by utilizing not only the absorption properties of X-rays but also the refraction and scatter rejection (extinction) properties. In this study, analyser-based computed tomography has been implemented on imaging an articular cartilage sample, depicting substructural variations, without overlay, at a pixel resolution of 3.6 μm.

Keywords: cartilage; analyser-based imaging; computed tomography.

1. Introduction

For imaging purposes from the early days of Wilhelm Conrad Röntgen's discovery up to nearly 100 years later, only the attenuation of an X-ray beam, caused by absorption, while passing through an object was used. Aside from absorption though, phase modulations of an X-ray beam transversing an object may also be employed for imaging purposes. Imaging methods using this latter approach are known as X-ray phase-contrast imaging (PCI) methods. PCI methods include further imaging subgroups, among which the analyser-based (AB) imaging method employs a perfect crystal for transforming angular phase deviations into intensity variations used to visualize the object being scanned (Forster *et al.*, 1980; Podurets *et al.*, 1989).

In the last decade, numerous studies have been performed showing the benefit of AB imaging in various fields (Kelly *et al.*, 2007; Yin *et al.*, 2005; Liu *et al.*, 2007; Fernandez *et al.*, 2005). Using diffraction-enhanced (DE) imaging, in principle an AB imaging technique that applies a dedicated algorithm for image reconstruction developed by Chapman *et al.* (1997), the group of Wagner *et al.* (2006) have shown that DE images can depict bony in-growth into the hydroxyapatite layer of implants, and may therefore be a useful tool for the diagnosis and understanding of implant healing and/or loosening.

Particularly for the field of cartilage research, AB imaging promises to be a powerful alternative to currently available methods such as X-ray- or magnetic-resonance-based techniques. Owing to the low X-ray absorption properties of cartilage, X-ray-based imaging, such as found in conventional radiography or in computed tomography (CT), fails to visualize cartilage directly.

In recent years, magnetic resonance (MR) imaging has evolved as an invaluable diagnostic method in the evaluation of cartilage pathologies such as osteoarthritis (Hunter *et al.*, 2008; Ding *et al.*, 2008). Using MR imaging visualization of the gross cartilage morphology is accurately possible (Kraff *et al.*, 2007; Siepmann *et al.*, 2007), but MR sequences capable of depicting early alterations within the cartilage matrix before gross morphological variations occur are still under development (Alhadlaq *et al.*, 2004; Kurkijarvi *et al.*, 2008).

This is where AB imaging can provide additional information. In an *ex vivo* study on human tali, Li *et al.* (2005) were able to visualize all stages of cartilage lesion associated with osteoarthritis (which range from fibrillation to erosion). They showed a high inter-observer agreement (κ = 0.93) between the DE images and the gross macroscopic grading even for early-stage changes of osteoarthritis, where MR imaging often finds its limitation in diagnostic specificity. Using an *in situ* animal model, Muhleman *et al.* (2006) were able to differentiate different stages of cartilage lesions (from normal through erosion down to the bone surface) within anatomical intact canine knee joints. In an effort to take imaging one step further based on Benninghoff's model, which states that the collagen fibers in cartilage bundle in arcades (resembling gothic columns) and divide the cartilage into four zones, the so-called calcified, deep, transitional and superficial zones, Muehleman *et al.* (2004) were able to depict structural orientation and visualized vertical striations and arcades resembling variations within human tali and femoral head specimens.

In these cited, and most other previous, cartilage AB imaging studies though, radiographical approaches have been used. In principle, all radiographic imaging techniques merge the data of a whole object volume into a single two-dimensional image, generating an overall superimposed image. Internal and external structural variations cannot therefore be differentiated. In order to generate an image that gives a true

account of the three-dimensional structure of the object, tomography techniques need to be used. A multitude of studies on DE computed tomography have been performed (Gao *et al.*, 2006; Sun *et al.*, 2007; Yuasa *et al.*, 2007; Bravin *et al.*, 2007; Huang *et al.*, 2007; Fiedler *et al.*, 2004), and Hashimoto *et al.* (2006) have performed a three-dimensional reconstruction of a mouse claw observing articular cartilage as well as bony structures such as trabeculae and marrow.

However, to the best of our knowledge, no AB computed tomography study has yet focused on solely depicting cartilage and its substructures. The aim of our study was to implement and introduce AB computed tomography for cartilage imaging as an alternative, and in principle non-destructive, technical approach to visualizing substructural variations within the cartilagenous matrix.

2. Material and methods

2.1. Specimen

Using a standard bone biopsy needle, an unfixed cartilage specimen (2.6 mm diameter) was obtained from a fresh human cadaver tibial plateau of a body donor to the Institute of Anatomy, Campus Mitte, Charité Universitaetsmedizin Berlin, Germany. Prior to death the donor had given a personally signed consent to dedicate his body to research. For storage purposes the specimen was refrigerated (281 K) in a saline solution before the scanning, whereas during the scanning a custom-built holder, with a duroplastic plastic cover to prevent the specimen from drying out, was used. A stable and fixed holding of the specimen using wax for fixation was assured after several testings.

2.2. AB computed tomography

Measurements were carried out at the Synchrotron Refraction Computed Tomography Unit of the Materials Research Laboratory (BAMline) of the Federal Institute for Materials Research and Testing (BAM) at the Berlin Electron Storage Ring for Synchrotron Radiation (BESSY). The usable photon energy range of the beamline extends from 5 keV up to 60 keV for monochromatic radiation. A parallel and monochromatic beam (30 mm horizontal and 5 mm vertical width) set to a photon beam energy of 20 keV was delivered by a double-crystal monochromator (DCM). The beam from the DCM was then reflected by two Si(111) single crystals in a symmetric configuration. They were set to their Bragg condition for the chosen energy. An X-ray-sensitive CCD camera was placed behind the second crystal, detecting the photons diffracted by the second crystal with a lateral resolution of about 3.6 μm × 3.6 μm. Different from the set-up for propagation phase-contrast CT, the specimen was situated in the X-ray beam between the two crystals. The rocking-curve width of the second crystal against the first crystal was 1.4×10^{-4} deg full width at half-maximum (FWHM). The highly collimated and monochromated beam from the first crystal was transmitted through the specimen and, according to the absorption properties of the specimen, the beam was then attenuated. Additionally, the beam was deflected owing to the refraction effect at all interfaces in the specimen as explained elsewhere (Mueller *et al.*, 2003). This led to a broadening of the rocking curve to 1.8×10^{-4} deg FWHM. The scan was performed with the second crystal set to the maximum of the rocking curve leading to a maximum rejection of all refracted and scattered X-rays caused by the interfaces inside the specimen. During the measurement the specimen was rotated around its cylinder axis for 180° in steps of 0.3° and with exposure times of 7 s. The data sets were then analyzed by filtered back-projection for parallel-beam conditions as known from data post-processing in conventional absorption CT.

After the AB computed tomography scan, histological sections of the specimen were prepared and stained with haematoxylin and eosin solution.

3. Results

Representative images and sections of the AB computed tomography results are presented in Fig. 1. A heterogeneous texture of the cartilage is revealed with hypodense areas ubiquitously distributed in the main matrix. A more vertical alignment of the hypodensities is present in about two-thirds of the cartilage on the sagittal reconstruction. Upon histological sectioning of the specimen, one can identify a multitude of chondrocytes within the main cartilage matrix as shown in an enlarged section (Fig. 2).

4. Discussion

To the best of our knowledge this is the first study to visualize structural variations within cartilage using AB computed tomography. The strength of our results lay in the fact that the

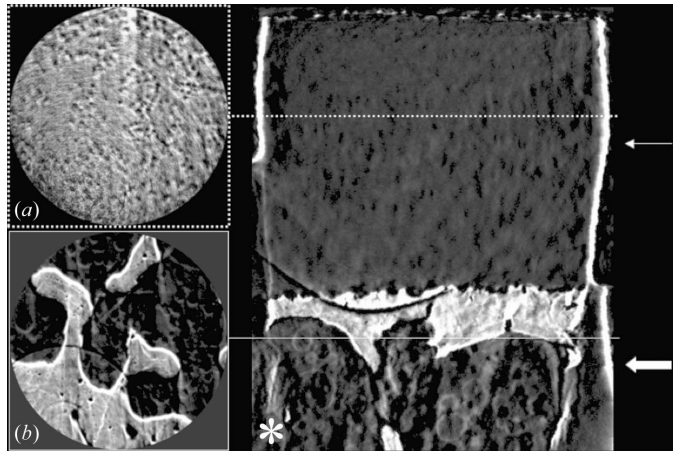

Figure 1
AB computed tomography image of the cartilage specimen. In (*a*) and (*b*) axial sections in different heights of the specimen are shown. Note the lines in the sagittal reconstruction (*). Hypodense areas within the homogeneous main cartilage matrix are clearly depicted in (*a*), whereas in (*b*) subchondral bone, trabecular bone and bone marrow vacuoles (thick white arrow) can be identified. A more vertical alignment of the hypodensities in about two-thirds of the cartilage can be seen upon sagittal reconstruction (*).

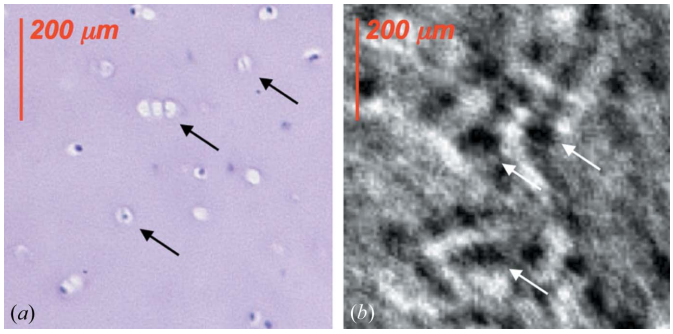

Figure 2
Enlarged section from the histology (*a*) and AB computed tomography (*b*) of the scanned cartilage specimen. On the histological section the chondrocyte lacunes are marked with black arrows. On the AB computed tomography reconstruction the overall depicted hypodense areas are marked with white arrows.

presented structural variations are depicted without overlay, proposing that what is shown is a representative image of the cartilaginous matrix. In addition, we further strongly hypothesize that the hypodensities we have depicted represent chondrocyte lacunes. Undeniably though, comparative studies on this matter need to be undertaken in the future, as our experimental set-up lacks an adequate section registration.

In addition, it needs to be proven as to whether or not the more vertical orientation of the hypodensities can be understood as an effect of the overall collagen fibre alignment. Even though, at this point in time, AB computed tomography is a modality used in only a limited number of facilities, we believe that for the understanding of cartilage pathologies such as osteoarthritis it holds a strong potential in imaging substructural changes that are invisible to alternative techniques. With our current study, we aimed to introduce and focus on the benefits of AB computed tomography for cartilage imaging, and in the long term hope to evaluate a model describing the substructural changes that occur in cartilage pathologies and furthermore to develop quantitative measures enabling structural analysis of cartilaginous tissue based on analyser-based imaging.

References

Alhadlaq, H. A., Xia, Y., Moody, J. B. & Matyas, J. R. (2004). *Ann. Rheum. Dis.* **63**, 709–717.

Bravin, A., Keyrilainen, J., Fernandez, M., Fiedler, S., Nemoz, C., Karjalainen-Lindsberg, M. L., Tenhunen, M., Virkkunen, P., Leidenius, M., von Smitten, K., Sipila, P. & Suortti, P. (2007). *Phys. Med. Biol.* **52**, 2197–2211.

Chapman, D., Thomlinson, W., Johnston, R. E., Washburn, D., Pisano, E., Gmur, N., Zhong, Z., Menk, R., Arfelli, F. & Sayers, D. (1997). *Phys. Med. Biol.* **42**, 2015–2025.

Ding, C., Cicuttini, F. & Jones, G. (2008). *Nat. Clin. Pract. Rheumatol.* **4**, 4–5.

Fernandez, M., Keyrilainen, J., Serimaa, R., Torkkeli, M., Karjalainen-Lindsberg, M. L., Leidenius, M., von Smitten, K., Tenhunen, M., Fiedler, S., Bravin, A., Weiss, T. M. & Suortti, P. (2005). *Phys. Med. Biol.* **50**, 2991–3006.

Fiedler, S., Bravin, A., Keyrilainen, J., Fernandez, M., Suortti, P., Thomlinson, W., Tenhunen, M., Virkkunen, P. & Karjalainen-Lindsberg, M. (2004). *Phys. Med. Biol.* **49**, 175–188.

Forster, E., Goetz, K. & Zaumseil, P. (1980). *Krist. Tech.* **15**, 937–945.

Gao, X., Luo, S., Yin, H., Liu, B., Xu, M., Yuan, Q., Gao, X. & Zhu, P. (2006). *Comput. Med. Imaging Graph.* **30**, 339–347.

Hashimoto, E., Maksimenko, A., Sugiyama, H., Hyodo, K., Shimao, D., Nishino, Y., Ishikawa, T. & Ando, M. (2006). *Zoolog. Sci.* **23**, 809–813.

Huang, Z. F., Kang, K. J., Zhu, P. P., Huang, W. X., Yuan, Q. X. & Wang, J. Y. (2007). *Phys. Med. Biol.* **52**, 1–12.

Hunter, D. J., Lo, G. H., Gale, D., Grainger, A. J., Guermazi, A. & Conaghan, P. G. (2008). *Ann. Rheum. Dis.* **67**, 206–211.

Kelly, M. E., Coupal, D. J., Beavis, R. C., Schultke, E., Romanchuk, K., Juurlink, B. H., Zhong, Z. & Chapman, L. D. (2007). *Can. J. Ophthalmol.* **42**, 731–733.

Kraff, O., Theysohn, J. M., Maderwald, S., Saylor, C., Ladd, S. C., Ladd, M. E. & Barkhausen, J. (2007). *Rofo Fortschr. Geb. Rontgenstr. Bildgeb. Verfahr.* **179**, 1231–1235.

Kurkijarvi, J. E., Nissi, M. J., Rieppo, J., Toyras, J., Kiviranta, I., Nieminen, M. T. & Jurvelin, J. S. (2008). *Magn. Reson. Imaging.* **26**, 602–607.

Li, J., Williams, J. M., Zhong, Z., Kuettner, K. E., Aurich, M., Mollenhauer, J. & Muehleman, C. (2005). *Osteoarthritis Cartilage*, **13**, 187–197.

Liu, C., Yan, X., Zhang, X., Yang, W., Peng, W., Shi, D., Zhu, P., Huang, W. & Yuan, Q. (2007). *Phys. Med. Biol.* **52**, 419–427.

Muehleman, C., Li, J. & Zhong, Z. (2006). *Osteoarthritis Cartilage*, **14**, 882–888.

Muehleman, C., Majumdar, S., Issever, A. S., Arfelli, F., Menk, R. H., Rigon, L., Heitner, G., Reime, B., Metge, J., Wagner, A., Kuettner, K. E. & Mollenhauer, J. (2004). *Osteoarthritis Cartilage*, **12**, 97–105.

Mueller, B. R., Lange, A. & Hentschel, M. P. (2003). *Synchrotron Radiation Refraction Topography*. Berlin: Springer.

Podurets, K. M., Somenkov, V. A. & Shil'shtein, S. S. (1989). *Sov. Phys. Tech. Phys.* **34**, 654–657.

Siepmann, D. B., McGovern, J., Brittain, J. H. & Reeder, S. B. (2007). *AJR Am. J. Roentgenol.* **189**, 1510–1515.

Sun, Y., Zhu, P., Yu, J. & Chen, X. (2007). *Comput. Med. Imaging Graph.* **31**, 383–389.

Wagner, A. *et al.* (2006). *Phys. Med. Biol.* **51**, 1313–1324.

Yin, H., Gao, X., Luo, S., Liu, B., Gao, X., Zhu, P. & Shu, H. (2005). *Conf. Proc. IEEE. Eng. Med. Biol. Soc.* **6**, 5699–5701.

Yuasa, T., Maksimenko, A., Hashimoto, E., Akatsuka, T. & Ando, M. (2007). *Conf. Proc. IEEE Eng. Med. Biol. Soc.* **1**, 4441–4444.